JOURNAL OF SPACECRAFT AND ROCKETS
Vol. 38, No. 4, July–August 2001

Effects of Boattailing on the Turbulence Structure of a Compressible Base Flow

C. J. Bourdon* and J. C. Dutton†
University of Illinois at Urbana–Champaign, Urbana, Illinois 61801

The large-scale turbulent structures in the near wake of a boattailed, axisymmetric afterbody immersed in a supersonic flow are examined using a planar Mie/Rayleigh scattering visualization technique. Seven key regions in the near wake are studied in both side- and end-view orientations. Estimates of the mean structure size, shape, and inclination are made using spatial correlation analysis, and the effects of the turbulent structures' passage are measured via steadiness and convolution analysis techniques. The results indicate that base drag is decreased by afterbody boattailing because the turbulent structures are generally less active in the separated flow region, and, as a result, shear-layer growth is suppressed. The latter result occurs because the large-scale turbulent structures are further inclined down toward the mean flow direction and tend to be organized more in the streamwise than in the spanwise direction near the base.

Nomenclature

A	=	area
A, B, BC, C, D, DE, E	=	imaging positions
a	=	major axis
b	=	minor axis
h	=	horizontal
M	=	Mach number
M_c	=	convective Mach number
Re	=	Reynolds number
r	=	radius
x, y, z	=	cardinal axes
β	=	body surface angle
δ	=	shear-layer thickness

Subscripts

base	=	property of the base
cen	=	relative to the end-view centroid
end	=	end view
local	=	local property
r	=	reattachment
side	=	side view

Superscript

$'$	=	fluctuation

Introduction

THE primary goal of this work is to characterize the nature and structure of the organized turbulence present in the separated flow region immediately following the termination of a boattailed afterbody in a supersonic flow. A detailed schematic of the flow is given in Fig. 1. There are many features that complicate the nature of the organized turbulence in such a flow. These include expansion fans that form at both the boattail junction with the body and at the base corner, recompression shocks that form as the separated shear layer approaches the symmetry axis, and a strong recirculation region located immediately adjacent to the base. It is because of the interaction of these features with the organized turbulence that computer modeling of such flows is quite challenging.[1,2] For this reason it is critical that experimental studies continue to explore base flows of various geometries and with different turbulence characteristics.

Great strides have been made in improving the drag characteristics of missiles and projectiles by modifying the base geometry.[3–5] Boattailing, or introducing a constant body surface angle β prior to separation (Fig. 1), has been shown to significantly increase base pressure (and thus reduce base drag). Several researchers[4,6,7] have empirically established the effects of boattailing on base pressure for varying boattail angles, Mach numbers, and Reynolds numbers. A recent study by Herrin and Dutton[8] has taken this research a step further, using laser Doppler velocimetery (LDV) to characterize the effects of boattailing on the near-wake velocity field. This study showed that, in addition to reducing the overall base drag by 17% for the current boattailed geometry, the shear-layer growth rate is reduced by 20%, and peak turbulence levels are significantly reduced (18% reduction in peak turbulent kinetic energy) compared to the blunt-base case.[8,9] These authors concluded that the decreased levels of turbulence in the preseparation boundary layer and the decreased strength of the expansion at separation cause these differences. Further investigation[10] has shown that, although decreased expansion strength reduces the overall turbulence level in the shear layer, it does not significantly alter the "turbulence structure" downstream of the expansion, i.e., the relative distribution of turbulence energy between the Reynolds stress components is relatively unaffected.

LDV and hot-wire anemometry provide critical information about the mean and rms velocities of a flow, but the point-wise nature of the measurements generally limits their ability to examine the large-scale turbulence structure present in shear flows. Essentially, the passage of a large-scale structure is indicated in the velocity data gathered by these techniques, but rigorous information about the nature of the turbulent structure itself is not. Particle image velocimetry provides planar velocity measurements, but the complexities of seeding a compressible, reattaching flow are many and have prohibited its past use in flows of this type.[11–13] Thus, although these techniques improve our understanding of base flows, they are incapable of visualizing and completely characterizing the turbulence structure in the base region.

For these reasons flow-visualization techniques are necessary to obtain information about the coherent structures present in compressible base flows. Because both the gross flow geometry and the turbulence structure organization are not planar in nature, any visualization technique that is used must either yield three-dimensional visualizations or illuminate multiple thin slices of the flowfield to resolve the three-dimensional features of the turbulence. For the thermodynamic conditions present in the current flow facility, a planar Mie scattering visualization technique that relies on

Received 25 July 2000; revision received 5 March 2001; accepted for publication 6 March 2001.

*Graduate Research Assistant, MC-244, Department of Mechanical and Industrial Engineering, 1206 West Green Street. Student Member AIAA.

†W. Grafton and Lillian B. Wilkins Professor, MC-244, Department of Mechanical and Industrial Engineering, 1206 West Green Street. Associate Fellow AIAA.

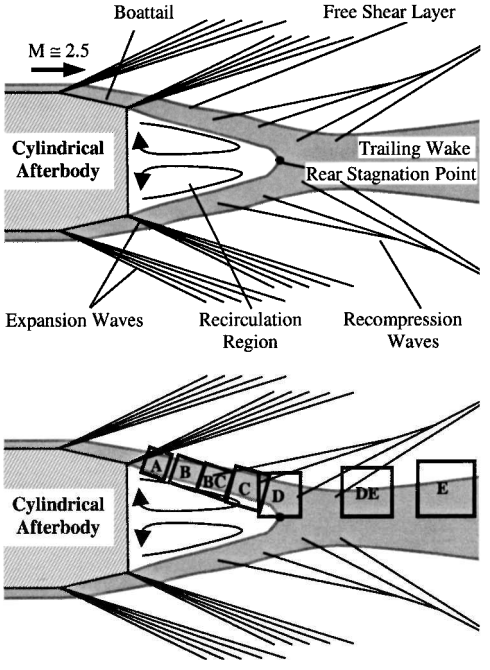

Fig. 1 Schematic of mean near-wake flowfield and imaging positions behind boattailed afterbody.

the condensation of ethanol[14] has proven its value in studying the turbulent structures present. This planar Mie scattering technique is used to visualize the interface between the freestream and recirculation/wake core fluids, and spatial correlation, steadiness, and shape factor analyses are applied to images recorded at key locations in the flowfield. From these analysis techniques information is gained about the mean size, eccentricity, and orientation of the turbulent eddies present in the shear layer; about the instantaneous position and enclosed end-view area of the core fluid; and about the degree of convolution of the freestream/core fluid interface.

Flow Facility

These experiments were performed in the axisymmetric base flow facility at the University of Illinois at Urbana—Champaign. The mean freestream Mach number is 2.46, and the unit Reynolds number is 52×10^6 m^{-1}. The freestream turbulence is quite low, less than 1%. Physical support for the afterbody base model is provided by a cylindrical sting that extends upstream through the nozzle to avoid any flow disturbances in the near wake. A more comprehensive description of the facility is given in Ref. 9.

The boattail implemented in the current study (Fig. 1) has a conical shape with a convergent angle of 5 deg in relation to the symmetry axis. The boattailing occupies the last 31.75 mm of the afterbody length or 1 base radius. This angle was chosen because it is near the optimal boattail angle given for minimum afterbody drag at Mach 2.5 (Ref. 4).

Instrumentation and Procedure

A challenge facing the current experiments was to find a technique that allows direct visualization of the large-scale turbulent structures that contain and convect the turbulent energy in a boattail flow. As already mentioned, Mie scattering from condensed ethanol droplets has been applied to accomplish this goal, as outlined by Clemens and Mungal.[14] This technique has been successfully applied to other base flows.[15–19] The thermodynamic characteristics of ethanol dictate that, given the stagnation conditions of the experimental facility, the ethanol vapor seeded into the freestream will condense at a Mach number above approximately unity.[20] Thus, the interface that is visualized separates the supersonic freestream from the subsonic recirculation and wake core regions.

The ethanol is injected at 0.23% mass fraction well upstream of the test section to ensure complete evaporation and uniform distribution in the freestream. The ethanol recondenses into a fine mist as the airflow is accelerated through the supersonic converging-diverging nozzle. The condensed ethanol droplet size has been estimated[20] to be approximately 0.05 μm, which is easily small enough to accurately follow the flow. A 200-μm-thick laser sheet illuminates the ethanol fog. The illumination is generated from a Nd:YAG laser beam that is formed into a sheet by a series of beam-shaping optics. A 14-bit unintensified charge-coupled device camera collects the scattered light. Figure 2 contains a schematic of the data-acquisition apparatus. Further information about the Mie scattering diagnostic and the saturation characteristics of ethanol can be found in Ref. 20.

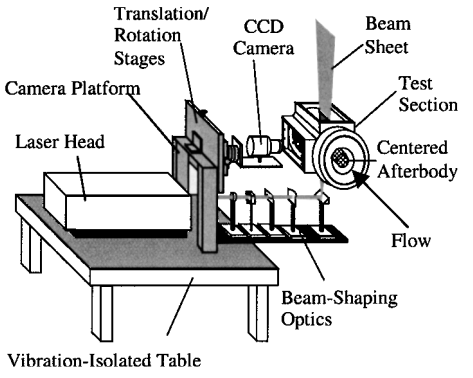

Fig. 2 Mie scattering image acquisition system.

From these images the mean size, shape, and eccentricity of the large-scale turbulent images can be determined through the use of a spatial correlation technique.[18] Flapping motions of the shear layer can also be determined,[19] and the degree of convolution or tortuousness of the interface between the freestream and core fluid can be examined.[19,21] The latter feature is related to the "mixing potential" between the recirculating and freestream flows.

Results and Discussion

Overall Features

Instantaneous global composite images of the near-wake region of the boattailed and blunt-based afterbodies are presented in Fig. 3. When comparing these two images,[18] several key differences are apparent. The recompression shock system appears much weaker in the boattail near-wake, such that individual shocks cause smaller light intensity changes in the images, if they are apparent at all. Because of the weaker recompression process in the boattail near-wake, the interface between the outer freestream and inner core fluid (i.e., the shear layer) demonstrates a smaller degree of curvature as it realigns with the symmetry axis. This interface appears to be much smoother in the present study than in the blunt-based near-wake region as well, indicating that turbulent structures are less active in the near-wake because of the afterbody boattail.

There are four distinct regions of interest in the near-wake flowfield: the postseparation shear layer (imaging positions A, B, and BC in Fig. 1), the recompression region (C), the reattachment region (D), and the trailing wake (DE and E). Each of these regions is characterized by various influences on the properties and turbulence structure of the shear layer. In the postseparation region the shear layer is dominated by velocity ratio and compressibility effects. The convective Mach number in this region is very high, nominally 1.35 (Table 1), indicating that the turbulence structure is highly three-dimensional and that interaction between the turbulent structures is suppressed. As the moniker suggests, the recompression region is characterized by an adverse pressure gradient, which is generated as the shear layer is turned along the streamwise axis. In the reattachment region the shear layer experiences the extra strain rates of lateral streamline convergence and concave streamline curvature as it approaches the symmetry axis. In the developing wake region the extra strain rates are relaxed, and the mean velocity along the centerline increases, so that the convective Mach number falls below 0.6. Therefore, two-dimensional instability modes and increased structure organization occur.

Seven locations have been chosen for image acquisition in the boattail near-wake flowfield (Fig. 1, bottom). These locations were

Table 1 Coordinates and flow parameters at imaging positions for boattail flow

Imaging position	Region	Distance from base corner, mm	Convective Mach number M_c	Mie scattering shear-layer thickness δ_{Mie}, mm	Mie scattering shear-layer angle, deg	End-view recirculation/wake core area (A_{mean}/A_{base})
A	Shear layer	19.1[a]	1.25	2.43	12.5	0.636
B	Shear layer	38.1[a]	1.43	3.31	14.0	0.484
BC	Shear layer	53.4[a]	1.36	3.49	12.5	0.254
C	Recompression	76.3[a]	1.22	3.64	8.6	0.130
D	Reattachment	89[b]	1.07	4.40	——	0.154
DE	Near wake	115.7[b]	0.67	6.04	——	0.082
E	Near wake	142.4[b]	0.42	7.58	——	0.032

[a]Measured from base corner. [b]Measured along centerline.

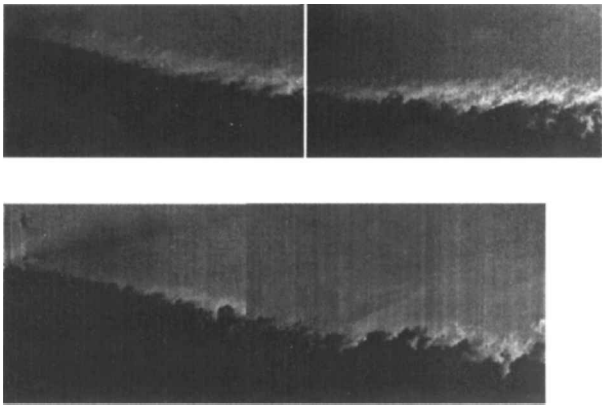

Fig. 3 Instantaneous global composite images of boattailed (top) and blunt-based (bottom) near-wake flowfields.

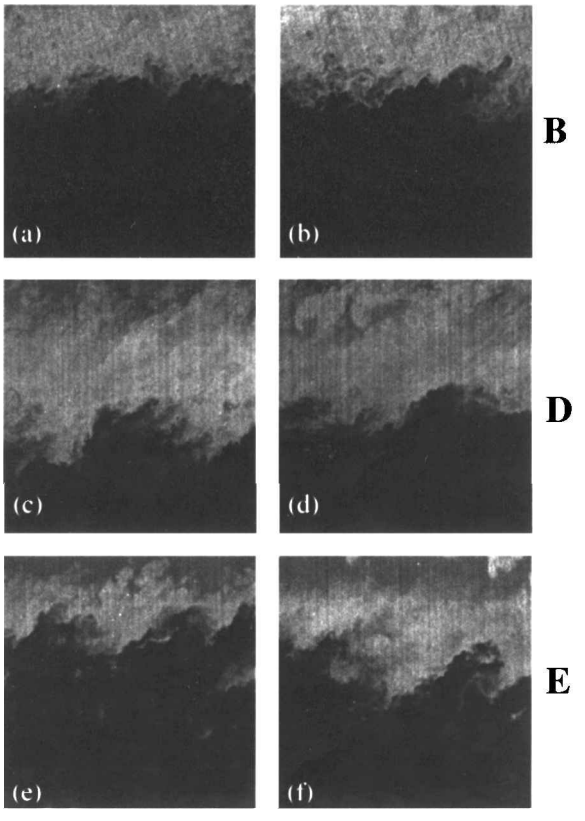

Fig. 4 Instantaneous side-view images from position B in the developing shear-layer region (a, b), position D in the reattachment region (c, d), and position E in the developing wake (e, f).

chosen to maximize understanding of the base flow by highlighting the varying influences in each region, as just described. Table 1 displays general data about the imaging locations, including position in relation to the base, local convective Mach number, shear-layer thickness, shear-layer angle in relation to the axis, and local end-view enclosed area. The imaging position labels (A, B, BC, etc.) have been assigned to correspond to the labels of past imaging studies.[15,18] Ensembles of approximately 500 images have been gathered at each imaging location in both side and end views. Ensembles of this size have been shown to be sufficient to produce stable statistics from the spatial correlation analysis.[15]

The general shape and orientation of the turbulent structures found along the freestream/core interface have been established previously for both planar[15] and axisymmetric[18] compressible, recirculating flows behind blunt-based afterbodies. The general features of the turbulent structures in the current boattail flowfield are qualitatively similar to earlier results: stringy, filamentlike structures in the side view, and ejection-type mushroom shapes in the end view. The side-view structures, as seen in preceding flows, are elliptical and/or polygonal and inclined toward the local flow direction. Sample instantaneous side- and end-view images are presented in Figs. 4 and 5 in the free shear layer (position B), reattachment (position D), and developing wake (position E) locations in the near wake. The primary difference between these and the preceding blunt-base image sets is the level of activity apparent in the images. Smaller-scale structures are much less visible for the boattail flow, and the largest scales present are much less strained and "violent" in appearance. The velocity measurements of Herrin and Dutton[8] support this conclusion with observations that the turbulent kinetic energy and shear-layer growth rate are substantially suppressed as a result of afterbody boattailing.

Shape Factor Analysis

The shape factor, a measure of the shear-layer convolution or tortuousness, is defined as the actual interface length in a given image divided by the corresponding minimum interface length (straight line in side views, circle in end views). The shape factor is slightly lower at all imaging locations (Fig. 6) in the boattailed afterbody case than in the blunt-base case in the side view, supporting the observation of less turbulence activity. In the end-view orientation (Fig. 7) both axisymmetric geometries possess roughly equal shape factors at all imaging locations, except in the trailing wake. Clearly, the insensitivity of the end-view shape factor to base geometry suggests that boattailing more significantly affects the streamwise turbulence structure than the circumferential (spanwise) structure seen in the end views. In agreement with this observation, it has been shown via LDV measurements[8] that the streamwise Reynolds normal stress is much more profoundly affected by the strength of the corner expansion, which is different for the blunt-base and boattail cases, than is the transverse normal stress.

Figure 8 presents a comparison of the number of large-scale structures visible, on average, at each end-view imaging location between the boattailed and blunt-based afterbody near-wake flowfields. This figure shows that in the initial stages of the shear layer, where it has not yet reached self-similar conditions,[22] there are approximately 20% more structures for the boattail case than for the blunt-base case. When the shear-layer thickness data of Table 1 are compared with the blunt-base data,[18] the shear-layer growth rate is found to be much lower for the boattail, just as found from LDV velocity data.[8] This result shows that there is less entrainment of fluid from the base region (and freestream) into the boattail shear layer, despite

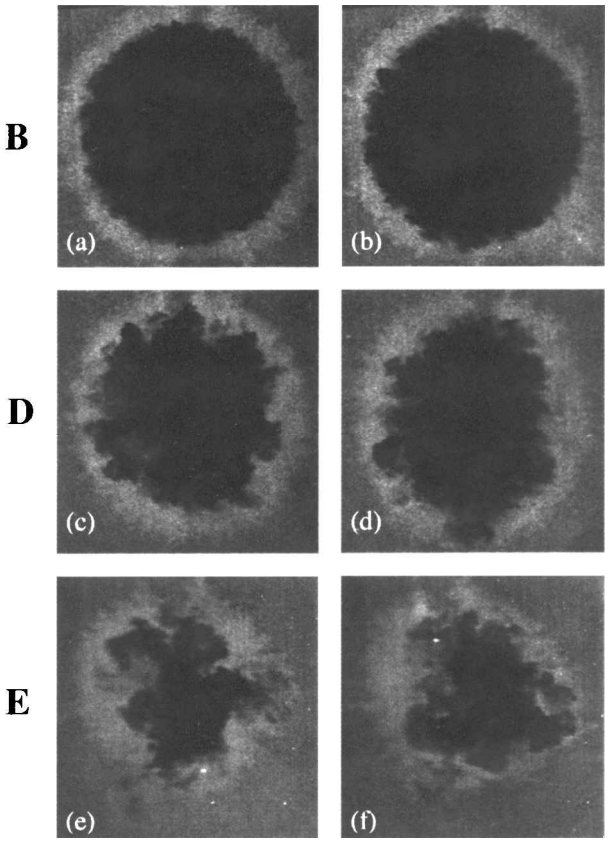

Fig. 5 Instantaneous end-view images from position B in the developing shear-layer region (a, b), position D in the reattachment region (c, d), and position E in the developing wake (e, f).

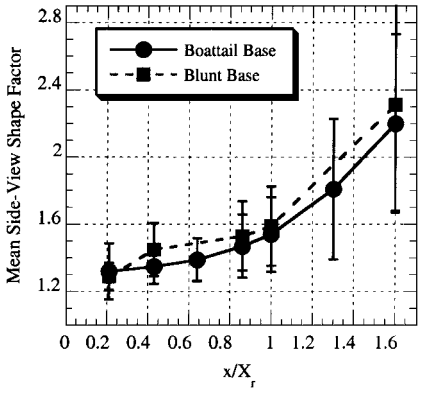

Fig. 6 Side-view shape factor for boattailed and blunt-based cases. Vertical bars denote rms shape factor values (i.e., one standard deviation).

the presence of a larger number of end-view turbulent structures. In turn, this reduced entrainment results in a higher base pressure (and lower base drag) for the boattailed afterbody.[8]

Shear-Layer Steadiness Analysis

The steadiness characteristics of the shear layer can be deduced from instantaneous images by monitoring the location of the interface between the freestream and core fluids. The interface is designated here as the location where the scattered light intensity drops to 20% of the peak value seen in the shear layer. The shear-layer position (normal to the streamwise direction) in each instantaneous side-view image can be compared with that of the entire ensemble, and bulk shear-layer motion can thus be detected. In the end view the shear layer is nominally a circular, closed curve. Because of this, both pulsing (or expansion/contraction) and flapping (or centroidal) motions can be described.

Figure 9 is a plot of the area-based fluctuations (normalized by the local mean area) seen in the end views of both the boattailed and

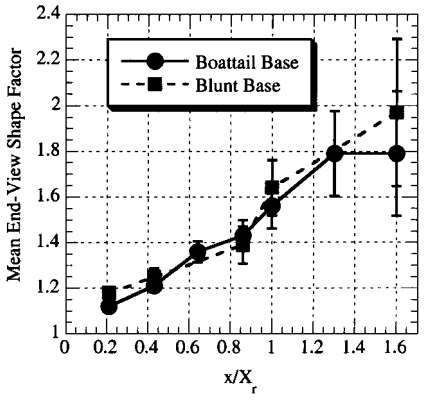

Fig. 7 End-view shape factor for boattailed and blunt-based cases. Vertical bars denote rms shape factor values (i.e., one standard deviation).

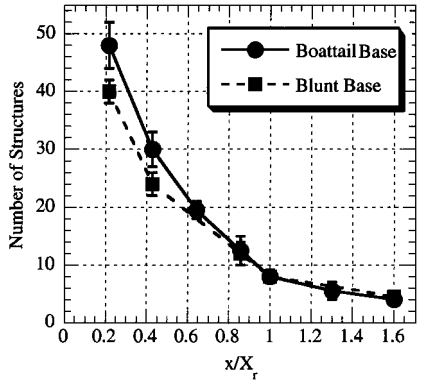

Fig. 8 Number of structures visible in the end-view orientation for boattailed and blunt-based cases. Vertical bars denote rms structure values (i.e., one standard deviation).

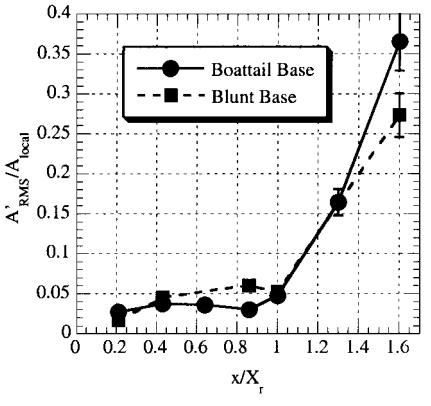

Fig. 9 RMS end-view area fluctuations normalized by the local mean end-view area. Vertical bars denote the statistical uncertainty of the measurements.

blunt-based flow geometries. Prior to the mean reattachment point, the area-based fluctuations are a relatively constant percentage of the local mean end-view area, approximately 4% for the boattailed geometry. This value is less than that seen in the blunt-based geometry at all but the position closest to the base. The lower level of end-view fluctuations in the boattail case suggests that the boattail expansion one base radius upstream of the base corner can reorient turbulence into axisymmetric modes that are quickly damped at downstream positions as a result of the high convective Mach number in this region. In agreement with this hypothesis, Herrin and Dutton[10] have shown that the overall turbulence level near the base is much lower in the boattail case than in the blunt-base case. They also indicate that the peak transverse Reynolds normal stress is initially higher for the boattail than the blunt-base case, but is quickly diminished to levels lower than for the blunt base slightly downstream. In a

similar vein several studies indicate that, as the convective Mach number increases above 0.6 for planar shear layers, the spanwise two-dimensional organization of the large-scale structures breaks down in favor of three-dimensional instability modes,[14,23–27] and the overall turbulence level decreases.[28,29]

In the developing wake the area-based fluctuations become significantly larger than prior to the mean reattachment point, caused primarily by the increasing role that the passage of a single structure has on the total core fluid area.[19] At the last imaging location (position E), Fig. 9 shows that the area fluctuations are significantly larger for the boattail geometry than the blunt-based geometry, but this result is slightly misleading. The local area of the wake core is significantly smaller in the boattail case than in the blunt-base case. Therefore, much smaller area fluctuations are necessary in the boattail case to provide large variations in $A'_{\mathrm{RMS}}/A_{\mathrm{local}}$. When normalized by the base area (constant), for instance, the area fluctuations are approximately four times smaller in the boattail case than in the blunt-based case.

Boattailing seems to dramatically decrease apparent end-view flapping motions, as demonstrated in Fig. 10 where the rms centroid position in the end views is plotted vs downstream position. Flapping motions increase monotonically with downstream distance in the boattail flowfield, unlike the flapping motions seen in planar (not shown) and axisymmetric blunt-based flowfields. The enhanced flapping seen in the recompression (position C) and wake-development regions (position E) caused by "sloshing" motion[19] for the blunt base is also missing in the boattail geometry. By viewing scatter plots of the instantaneous core fluid centroid location at these two positions (Fig. 11), it is apparent that such horizontal motions are not present in the boattail base flowfield. In contrast to the blunt-base geometry, the instantaneous centroid positions for the boattailed afterbody are roughly equally likely in any of the four

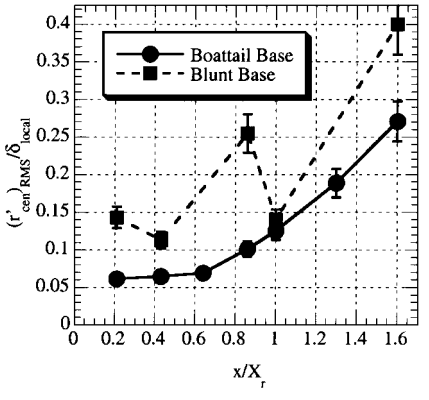

Fig. 10 RMS end-view centroid position fluctuations for boattailed and blunt-based cases. Vertical bars denote the statistical uncertainty of the measurements.

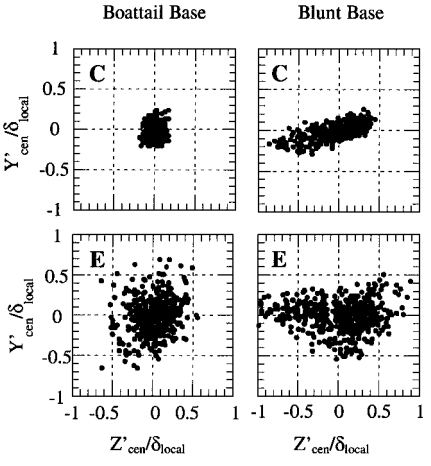

Fig. 11 End-view centroid positions at locations C and E in boattailed and blunt-based afterbody near-wake flowfields.

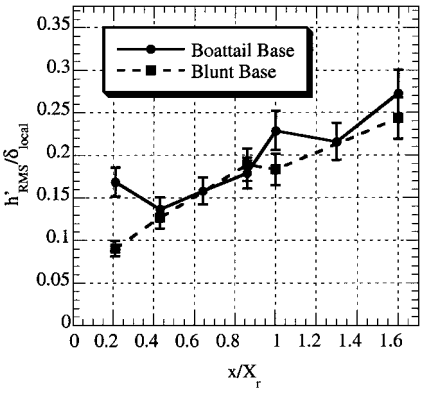

Fig. 12 RMS side-view shear layer position for boattailed and blunt-based afterbody near-wake flowfields. Vertical bars denote the statistical uncertainty of the measurements.

quadrants. In the blunt-base case the sloshing motion was linked to asymmetry in the organization of the large-scale structures at imaging locations C and E, which can be caused by the strong adverse pressure gradient (position C) and to the low convective Mach number (position E) present at these locations. The weaker recompression region in the current boattail flow configuration may have prevented such a phenomenon from occurring at position C, whereas the upstream disappearance of this phenomenon may prevent it from occurring in the wake region.

The rms magnitude of flapping motions (when normalized by the local shear-layer thickness) in the boattail geometry appears to be very similar to that for the blunt-based geometry when viewed from the side (Fig. 12). Key differences are evident near the base (position A) and at the mean reattachment point (position D) where the flapping motions correspond to a significantly larger percentage of the local shear-layer thickness for the boattail than for the blunt base. Increased side-view flapping motions near the base are consistent with the enhanced area-based fluctuations seen in the end views (Fig. 9). At the mean reattachment point the side-view flapping enhancement is most likely linked to the much smaller shear-layer thickness and proximity of the freestream/core interface to the symmetry axis for the boattail geometry. These factors enhance the sensitivity of the measurements to the passage of individual parcels of fluid from the base region into the developing wake.

Spatial Correlation Analysis

A spatial autocorrelation analysis technique, similar to that described by Messersmith and Dutton[26] and Smith and Dutton,[15] has been applied to large ensembles of images, such as those presented in Figs. 4 and 5. Objective information about the mean structure size, shape, and orientation can be gleaned from such an analysis, while limiting the subjectiveness of personal bias. Ensembles of approximately 500 images have been used in the spatial correlation analysis at each imaging position and for each orientation. The 0.5-correlation contour (where the central peak is normalized to a value of 1.0) has been previously established as the basis for determining the mean structure's characteristics.[15,16,18,19,26]

Figure 13 displays contour plots of the side-view correlation fields obtained at all seven imaging positions examined in this study. The image frames are sized such that the length of the vertical edge of the frame is approximately equal to the local shear-layer thickness. The contour levels have been chosen so that the outer contour is the 0.5 level, and successive contours increase in 0.1 intervals. All of the contour plots in this figure are oriented such that the local streamwise flow direction is horizontal and from left to right with the high-speed freestream on top. As seen in other related compressible shear flows,[15,18,26] the average structures are elliptical in shape and inclined toward the local flow direction. Prior to the recompression region, position C, the structures remain essentially "frozen," changing relatively little in size, shape, and orientation. The recompression process dramatically strains the structures in the streamwise direction, making the mean structures elongate and dip downward toward the local streamwise direction, much as seen in

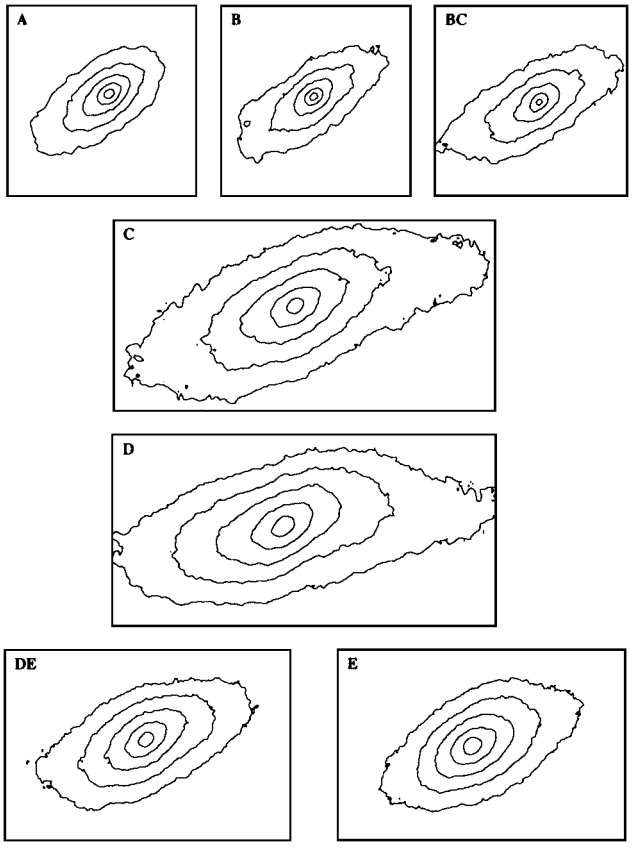

Fig. 13 Side-view correlation fields for all imaging locations. Contours are at 0.1 intervals from 0.5 to 0.9.

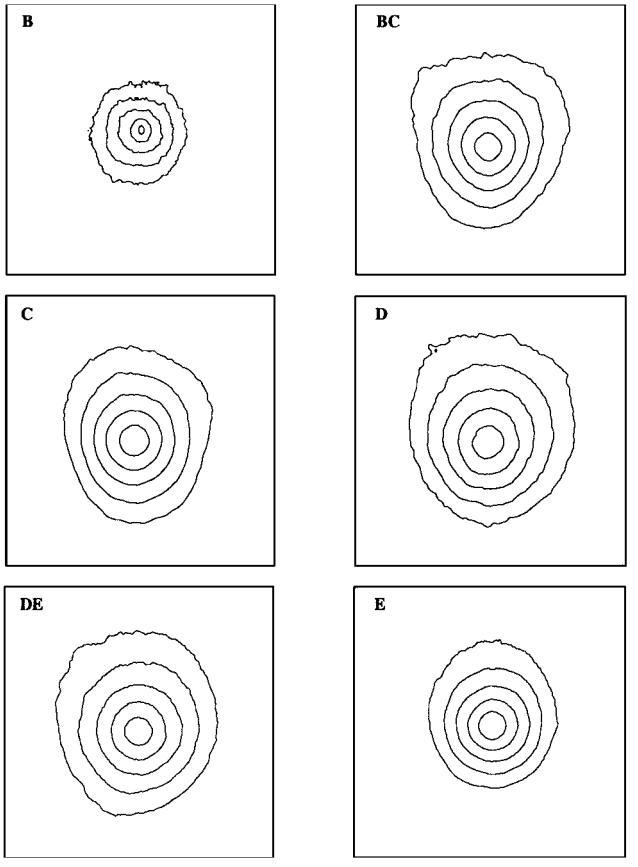

Fig. 14 End-view spatial correlation fields for imaging locations B–E. Contours are at 0.1 intervals from 0.5 to 0.9.

previous studies[15,18] of planar and axisymmetric blunt-base reattaching flows, respectively. In the developing wake (positions DE and E) the mean structures diminish in size and become less eccentric as the adverse pressure gradient vanishes and the convective Mach number decreases.

Another significant feature of the correlation field seen in previous studies[15,18] is the behavior of the angular orientation of the inner (higher correlation level) contours. Smith and Dutton[15] found that the inner contours tend to be rotated with respect to the 0.5 contour level in regions of the flow where adverse pressure gradients (destabilizing influence) act on the structures. They observed that contour rotation of this type occurs in the recompression (position C) and reattachment (position D) regions of a planar, reattaching base flow. Bourdon and Dutton[18] found similar results in their axisymmetric blunt-based reattaching flow, but further upstream in the trailing portion of the free shear-layer region (position B) and in the recompression region (position C), although not at the mean reattachment point. The absence of contour rotation at the mean reattachment point, where there is definitely an adverse pressure gradient, was attributed to the cancellation effect of lateral streamline convergence (stabilizing), which is present in the axisymmetric reattachment process but not in the planar reattachment process. Interestingly, in the present boattailed flow contour rotation is evident in the recompression and reattachment regions (positions C and D), but not farther upstream. The apparent similarity of these results to the planar (and not the blunt-based axisymmetric) geometries is explained by the weakened recompression process (higher base pressure) and elongated recirculation region caused by afterbody boattailing. The weakened recompression process limits the region over which the strong adverse pressure gradient acts. Thus, inner contour rotation is not evident at positions B or BC in the developing shear layer. The presence of contour rotation at the mean reattachment point (position D) indicates that, because of the decreased curvature of the streamlines in the vicinity of the mean reattachment point (as a result of the weakened recompression process and longer reattachment length), lateral streamline convergence effects are much weaker in the boattail geometry than in the blunt-based geometry.

The end-view correlation fields for positions B-E are presented in Fig. 14. These correlation contours are averages of spatial correlation fields computed with basis points located in the shear layer every 90 deg around its circumference. By doing this, the effects that can be caused by imperfections in the geometric transformation necessary to analyze the images as true end views can be limited. The correlation contours in Fig. 14 are oriented such that the recirculation/wake core region is at the bottom of the image frame, and the freestream is at the top. As in the axisymmetric blunt-based study,[18] the contours exhibit a wedge-like shape, with a slightly longer horizontal edge on the upper side than on the lower (most obvious at position BC). This is caused by axisymmetric confinement effects as the shear layer approaches the axis of symmetry.

The primary statistical results of the spatial correlation analysis of the images are presented in Figs. 15 and 16. All of the statistics presented herein correspond to the 0.5 correlation contours. There are some very critical differences between the boattail and blunt-base cases in the behavior of the average structures in the free shear-layer region near the base. The first of these is that the average structure at the first imaging location is much more inclined downward toward the local streamwise axis for the boattail: 35 vs 43 deg (Fig. 15c). Past researchers[15] have postulated that decreased structure angle is an indication of lower entrainment and mixing in the shear layer, which is consistent with the boattail's higher base pressure. The side-view correlation contours and instantaneous images of the structures also suggest that very little new generation or evolution of turbulent structures occurs in this region. Both the structure size (when normalized by the local shear-layer thickness) and angle remain virtually constant through the first two imaging positions for the boattail case, Figs. 15a and 15c.

The only statistic that does change significantly for the boattail geometry near the base is the end-view structure eccentricity (Fig. 16b). The angle of inclination of the shear layer with respect to the symmetry axis is lower for the boattail geometry than

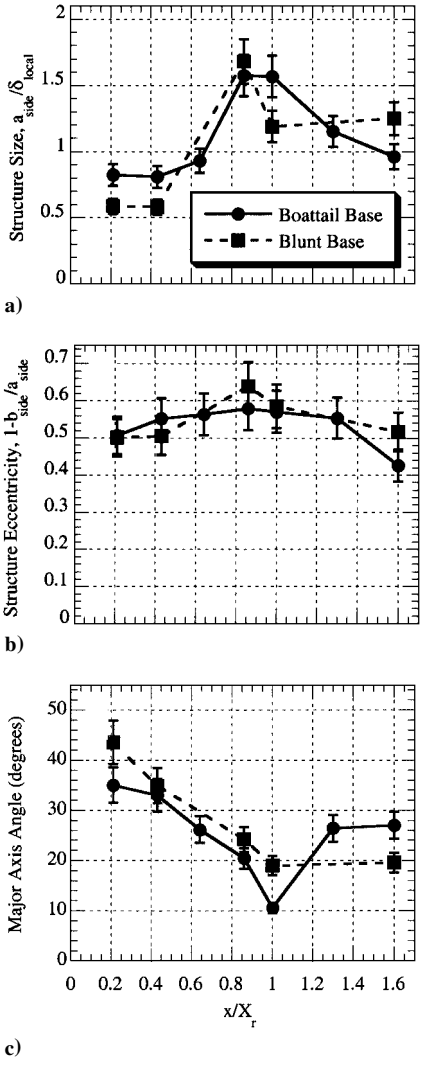

Fig. 15 Side-view correlation statistics at imaging locations A–E and for both boattailed and blunt-based afterbody near-wake flowfields. Vertical bars denote the statistical uncertainty of the respective measurements.

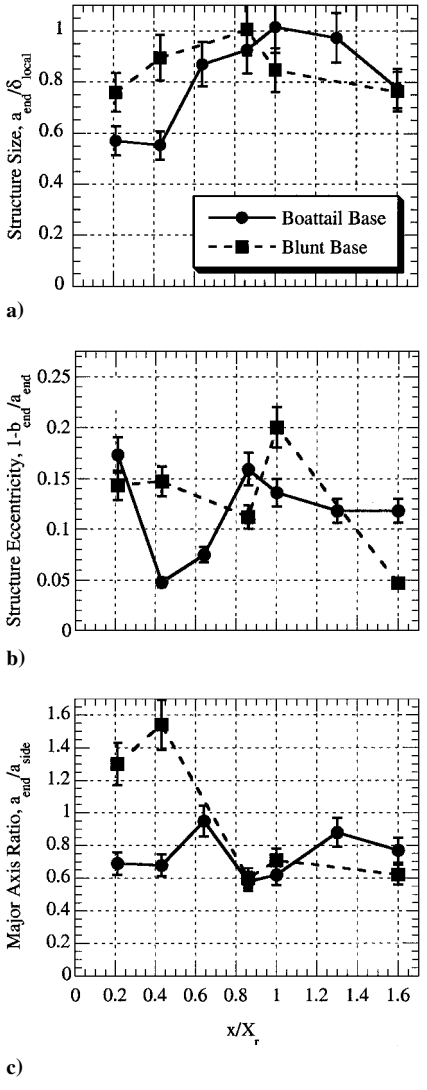

Fig. 16 End-view correlation statistics at imaging locations A–E and for both boattailed and blunt-based afterbody near-wake flowfields. Vertical bars denote the statistical uncertainty of the respective measurements.

the blunt-based geometry as a result of the elongated recirculation region. The elongated recirculation region also indicates that circumferential constriction effects are weaker, allowing the turbulent structures to acquire a more rounded, less eccentric shape in the end view.

LDV data[10] show that the peak normal stress anisotropy ratio is much higher initially in the blunt-base case than in the boattail case. As the shear layer develops toward a self-similar state, the peak normal stress values become approximately equal in the two flows. By examining the major axis ratio a_{end}/a_{side} (Fig. 16c), which can be used as a measure of the orientation of the dominant turbulence organization, the same trend is visible. Larger axis ratio values suggest a dominance in structure organization in the spanwise direction,[15] which also suggests the dominance of engulfment processes. Therefore, the boattailed afterbody inhibits the generation of engulfment-type motions in the initial portions of the shear layer. Further downstream of the base, where entrainment of recirculating fluid diminishes,[8] the major axis ratio for both axisymmetric cases and for a planar reattaching flow[15] all drop below unity, implying a dominance of structure organization in the streamwise direction.

In the recompression region (position C) the similarity between the behavior of the boattail and blunt-base flows is increased. The major axis ratio at the measurement location in this region, as well as at reattachment, is virtually identical for the two axisymmetric geometries, indicating similar organization of the turbulence field. In fact, in the recompression region all three studies (planar and axisymmetric) provide virtually identical results, despite differences in behavior farther upstream. The similar behavior of all three cases in the recompression region suggests that the effects of the adverse pressure gradient unify the behavior of the large-scale turbulent structures regardless of the geometry.

As the flow approaches the mean reattachment point, important differences are again seen in the results of the different geometries. Streamline convergence and axisymmetric confinement effects dictate a heightened organization in the end view of the blunt-base and boattail geometries (slightly increasing a_{end}/a_{side}, Fig. 16c), whereas in the planar case,[15] which is not subject to such effects, the structure organization continues to shift to streamwise (i.e., side-view) dominance. Both the blunt-base and boattailed axisymmetric cases indicate peaks in the side-view structure size prior to the mean reattachment point, Fig. 15a. The similarity of the side-view structure size measurements at imaging locations C and D (in the recompression and reattachment regions, respectively) for the boattailed afterbody suggests that the peak value may lie somewhere between these two points. This correlates well with LDV data in this region,[8] which do not show a dramatic drop-off in the peak axial Reynolds normal stress until just before the mean reattachment point. This drop-off occurs earlier in the blunt-based axisymmetric case.[9] The mean side-view structure angle, Fig. 15c, is also dramatically lower (50%) at reattachment for the boattail case than in both the planar and axisymmetric blunt-based cases, again implying lower entrainment of recirculation region fluid and higher base pressure for the boattail geometry.

Because of the relative weakness of the recompression and reattachment processes, some other noteworthy differences are present at the mean reattachment point caused by boattailing. The first of these is that the end-view structure size (Fig. 16a) is a maximum at the mean reattachment point, while it decreases from upstream values for both the planar and axisymmetric blunt-based geometries. A second observation is that the side-view structure eccentricity (Fig. 15b) is relatively constant throughout the recompression and reattachment processes for the boattail case, while peaking in the recompression region for the axisymmetric blunt-based case.

In the developing wake region the lower entrainment levels present downstream dictate that the shear layer is much thinner and the wake core area is much smaller in the boattail case than in the blunt-based case. The lower shear-layer thickness and smaller wake core area imply that, because the same number of structures is present in this region (Fig. 8) the turbulent structures occupy a larger percentage of the shear layer and core regions in the end view of the boattail geometry in the near wake. This spatial constraint, in turn, causes the structures to "sit up" more in the side view, leading to increased structure angle (Fig. 15c).

Conclusions

There are several key differences in the behavior of the turbulent structures present in blunt-based and boattailed axisymmetric supersonic base flows. The most prominent of these are in the initial shear layer formed immediately after separation. First, 20% more structures are visible in the end view near separation for the boattail case, and the structures are larger and more inclined downward toward the local flow direction in the side view. These factors indicate lower entrainment rates and thus higher base pressure. Second, boattailing causes a weakening of the preferential organization of the large-scale structures toward the end view immediately after separation. This organizational weakening in the end view indicates that ejection-type end-view motions are less prevalent, another indication of lower entrainment rates and higher base pressure. Third, despite differences seen upstream, the recompression process displays remarkably similar spatial correlation results for the planar, boattailed, and blunt-based axisymmetric geometries. This similarity in the recompression region suggests that in the absence of the strong influences of other extra rates of strain the adverse pressure gradient causes similar large-structure behavior regardless of upstream conditions. Fourth, the weakened recompression process in the boattail base flowfield leads to a larger streamline radius of curvature in the vicinity of the mean reattachment point (position D) and diminished streamline convergence strain-rate effects. The weakened recompression effects are evident in the side view as enhanced rms shear-layer position (flapping) and structure size in the boattail base case over the blunt-base case. In the end view the lowered streamline convergence effects lead to a peak structure size at reattachment, position D, for the boattail case. Fifth, in the developing wake region (positions DE and E), evidence remains of the differences in the upstream dynamics of the blunt base and boattail geometries. For instance, in the side view, the mean turbulent structures maintain a larger angle with respect to the symmetry axis in the developing wake because of spatial limitations placed on the structures by lower entrainment in the separated flow region (positions A–C).

Acknowledgments

Funding for this research was provided through the U.S. Army Research Office, Grant DAAG55-97-1-0122, with Thomas L. Doligalski as Technical Monitor.

References

[1]Sahu, J., "Numerical Computations of Supersonic Base Flow with Special Emphasis on Turbulence Modeling," *AIAA Journal*, Vol. 32, No. 7, 1994, pp. 1547–1549.

[2]Chuang, C. C., and Chieng, C. C., "Supersonic Base-Flow Computation Using Higher-Order Closure Turbulence Models," *Journal of Spacecraft and Rockets*, Vol. 33, No. 3, 1996, pp. 374–380.

[3]Rubin, D. V., Brazzel, C. E., and Henderson, J. H., "The Effects of Jet Plume and Boattail Geometry on Base and Afterbody Pressures of a Body of Revolution at Mach Numbers of 2.0 to 3.5," U.S. Army Missile Command, RD-TR-70-5, Redstone Arsenal, AL, 1970.

[4]Addy, A. L., and White, R. A., "Optimization of Drag Minimums Including Effects of Flow Separation," *Journal of Engineering for Industry*, Vol. 95, No. 1, 1973, pp. 360–364.

[5]Mathur, T., and Dutton, J. C., "Velocity and Turbulence Measurements in a Supersonic Base Flow with Mass Bleed," *AIAA Journal*, Vol. 34, No. 6, 1996, pp. 1153–1159.

[6]Reid, J., and Hastings, R. C., "The Effect of a Central Jet on the Base Pressure of a Cylindrical After-Body in a Supersonic Stream," Royal Aircraft Establishment, RAE Rept. Aero. 2628, Farnborough, England, U.K., Dec. 1959.

[7]Viswanath, P. R., and Narasimha, R., "Two-Dimensional Boat-Tailed Bases in Supersonic Flow," *Aeronautical Quarterly*, Vol. 25, No. 3, 1974, pp. 210–224.

[8]Herrin, J. L., and Dutton, J. C., "Supersonic Near-Wake Afterbody Boattailing Effects on Axisymmetric Bodies," *Journal of Spacecraft and Rockets*, Vol. 31, No. 6, 1994, pp. 1021–1028.

[9]Herrin, J. L., and Dutton, J. C., "Supersonic Base Flow Experiments in the near Wake of a Cylindrical Afterbody," *AIAA Journal*, Vol. 32, No. 1, 1994, pp. 77–83.

[10]Herrin, J. L., and Dutton, J. C., "Effect of a Rapid Expansion on the Development of Compressible Free Shear Layers," *Physics of Fluids*, Vol. 7, No. 1, 1995, pp. 159–171.

[11]Molezzi, M. J., and Dutton, J. C., "Study of Subsonic Base Cavity Flowfield Structure Using Particle Image Velocimetry," *AIAA Journal*, Vol. 33, No. 2, 1995, pp. 201–209.

[12]Olsen, M. G., and Dutton, J. C., "Planar Velocity Measurements in Incompressible Mixing Layers," American Society of Mechanical Engineers, FEDSM98-5254, June 1998.

[13]Olsen, M. G., and Dutton, J. C., "Planar Velocity Measurements in a Weakly Compressible Mixing Layer," AIAA Paper 99-3584, June 1999.

[14]Clemens, N. T., and Mungal, M. G., "A Planar Mie Scattering Technique for Visualizing Supersonic Mixing Flows," *Experiments in Fluids*, Vol. 11, No. 2, 1991, pp. 175–185.

[15]Smith, K. M., and Dutton, J. C., "Investigation of Large-Scale Structures in Supersonic Planar Base Flows," *AIAA Journal*, Vol. 34, No. 6, 1996, pp. 1146–1152.

[16]Smith, K. M., and Dutton, J. C., "Evolution and Convection of Large-Scale Structures in Supersonic Reattaching Shear Flows," *Physics of Fluids*, Vol. 11, No. 6, 1999, pp. 2127–2138.

[17]Boswell, B. A., and Dutton, J. C., "Flow Visualizations and Measurements of a Three-Dimensional Supersonic Separated Flow," *AIAA Journal*, Vol. 39, No. 1, 2001, pp. 113–121.

[18]Bourdon, C. J., and Dutton, J. C., "Planar Visualizations of Large-Scale Turbulent Structures in Axisymmetric Supersonic Separated Flows," *Physics of Fluids*, Vol. 11, No. 1, 1999, pp. 201–213.

[19]Bourdon, C. J., and Dutton, J. C., "Shear Layer Flapping and Interface Convolution in a Separated Supersonic Flow," *AIAA Journal*, Vol. 38, No. 10, 2000, pp. 1907–1915.

[20]Smith, K. M., "The Role of Large Structures in Compressible Reattaching Shear Flows," Ph.D. Dissertation, Dept. of Mechanical and Industrial Engineering, Univ. of Illinois, Urbana, IL, Aug. 1996.

[21]Glawe, D. D., Samimy, M., Nejad, A. S., and Chen, T. H., "Effects of Nozzle Geometry on Parallel Injection from Base of an Extended Strut into a Supersonic Flow," AIAA Paper 95-0522, Jan. 1995.

[22]Herrin, J. L., "An Experimental Investigation of Supersonic Axisymmetric Base Flows Including the Effects of Afterbody Boattailing," Ph.D. Dissertation, Dept. of Mechanical and Industrial Engineering, Univ. of Illinois, Urbana, IL, July 1993.

[23]Clemens, N. T., and Mungal, M. G., "Two- and Three-Dimensional Effects in the Supersonic Mixing Layer," *AIAA Journal*, Vol. 30, No. 4, 1992, pp. 973–981.

[24]Clemens, N. T., and Mungal, M. G., "Large-Scale Structure and Entrainment in the Supersonic Mixing Layer," *Journal of Fluid Mechanics*, Vol. 284, 1995, pp. 171–216.

[25]Elliott, G. S., Samimy, M., and Arnette, S. A., "The Characteristics and Evolution of Large-Scale Structures in Compressible Mixing Layers," *Physics of Fluids*, Vol. 7, No. 4, 1995, pp. 864–876.

[26]Messersmith, N. L., and Dutton, J. C., "Characteristic Features of Large Structures in Compressible Mixing Layers," *AIAA Journal*, Vol. 34, No. 9, 1996, pp. 1814–1821.

[27]Papamoschou, D., and Bunyajitradulya, A., "Evolution of Large Eddies in Compressible Shear Layers," *Physics of Fluids*, Vol. 9, No. 3, 1997, pp. 756–765.

[28]Goebel, S. G., and Dutton, J. C., "Velocity Measurements in Compressible Turbulent Mixing Layers," *AIAA Journal*, Vol. 29, No. 4, 1991, pp. 538–546.

[29]Elliott, G. S., and Samimy, M., "Compressibility Effects in Free Shear Layers," *Physics of Fluids A*, Vol. 2, No. 7, 1990, pp. 1231–1240.

M. S. Miller
Associate Editor